Ab Initio Derived Force Fields for Zeolitic Imidazolate Frameworks: MOF-FF for ZIFs

Johannes P. Dürholt,[†] Guillaume Fraux,[‡] François-Xavier Coudert,*,[‡] and Rochus Schmid*,[†]

[†]Computational Materials Chemistry group, Fakultät für Chemie und Biochemie, Ruhr-Universität Bochum, Bochum 44801, Germany

[‡]Chimie ParisTech, PSL University, CNRS, Institut de Recherche de Chimie Paris, 75005 Paris, France

S *Supporting Information*

ABSTRACT: In this paper, we parametrized in a consistent way a new force field for a range of different zeolitic imidazolate framework systems (ZIF-8, ZIF-8(H), ZIF-8(Br), and ZIF-8(Cl)), extending the MOF-FF parametrization methodology in two aspects. First, we implemented the possibility to use periodic reference data in order to prevent the difficulty of generating representative finite clusters. Second, a new optimizer based on the covariance matrix adaptation evolutionary strategy (CMA-ES) was employed during the parametrization process. We confirmed that CMA-ES, as a state-of-the-art black box optimizer for problems on continuous variables, is more efficient and versatile for force field optimization than the previous genetic algorithm. The obtained force field was then validated with respect to some static and dynamic properties. Much effort was spent to ensure that the FF is able to describe the crucial linker swing effect in a large number of ZIF-8 derivatives. For this reason, we compared our force field to ab initio molecular dynamic simulations and found an accuracy comparable to those obtained by different exchange−correlation functionals.
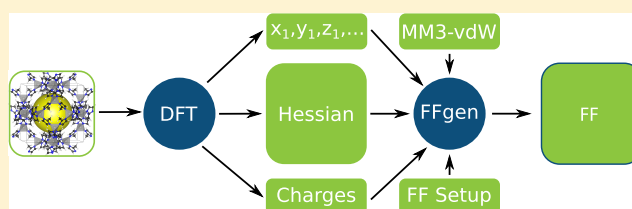
1. INTRODUCTION

Zeolitic imidazolate frameworks (ZIFs) are a subclass of metal−organic frameworks,[1−4] consisting of imidazolate linkers that bridge metal cations to form three-dimensional porous crystalline solids, which are isomorphous to zeolitic frameworks.[5] Like other MOFs, ZIFs are neither static nor rigid, and instead, they exhibit different types of flexibility. Flexibility in MOFs means that, upon external stimuli such as temperature, mechanical pressure, or guest molecule adsorption, the cell size and shape and, therefore, the pore size and geometry can change drastically—yet reversibly.[6,7] The most prominent example for flexibility in ZIFs is the so-called swing effect in ZIF-8. ZIF-8 is a low-density porous framework with the sodalite (**sod**) topology and chemical formula $Zn(mim)_2$, where *mim* = 2-methylimidazolate. The **sod** topology features large spherical cages separated by 6-ring windows of small aperture, and 4-rings that connect different cages (see Figure 5). By torsional motions of its imidazolate linkers, the frameworks can adsorb molecules with a kinetic diameter larger than its geometric window size.[8,9] It was recently shown by ab initio molecular dynamic simulations that functionalization of the organic linker can have a substantial influence on the swing effect.[10]

Furthermore, Mortada and co-workers were able to synthesize ZIF-8(Cl) and ZIF-8(Br), both in the **sod** topology employing 2-bromo and 2-chloroimidazolate as organic linkers. Interestingly they found that ZIF-8(Cl) exhibits a spring behavior with the highest amount of energy stored ever in high pressure intrusion-extrusion experiments.[11] These findings underline the potential of ZIFs for technical application. To exploit this potential, it is pivotal to gain an atomistic understanding of the underlying mechanisms, making molecular simulations a valuable tool and the accurate description of the frameworks' flexibility a crucial goal.

However, the use of periodic density functional theory (DFT) calculations and, in particular, DFT-based MD (also called ab initio MD) for such studies is limited to comparatively small length and time scales—because the computational cost increases very fast with both the size and number of atoms in the unit cell and the necessary sampling time. As long as bond breaking is not involved, less accurate molecular mechanics methods can be used to investigate larger systems for longer time scales. The difficulty is to define an energy expression that describes the relevant part of the potential energy surface with good accuracy and to determine the corresponding parameters. For computing the conformational flexibility of the porous MOF or ZIF matrix (as well as for the host−guest interactions, dominated by physisorption) conventional nonreactive force fields (FFs) that employ a separation in bonded and nonbonded terms, are a sufficiently good approximation.[12] However, the determination of parameters for the hybrid organic−inorganic part remains a challenging problem.

A frequently employed solution is to use so-called generic force fields, like UFF, where the parameters are generated by a

rule based system from a much smaller set of atomic parameters.[13] This allows the consistent treatment of a wide range of systems, including a number of MOFs, however, with a very limited and uncontrolled accuracy. This approach has recently been extended to MOFs, with the UFF4MOF extension of the UFF atomic parameter set.[14−16] For most of the computational studies dealing with ZIFs, the same approach was followed by combining generic force field parameters from UFF and AMBER, modified in an ad hoc manner to obtain experimentally observed properties. The drawback of this approach is 2-fold: first, the force fields obtained may not describe physical properties that were not considered in the adjustment procedure. Second, the manual adjustment may lead to the correct macroscopic observables, at the price of an unphysical microscopic picture. A brief overview of the published force fields dealing with ZIFs is given in the following paragraph.

In 2012, Jiang et al. developed a flexible force field for ZIF-8.[17] The equilibrium bond lengths and angles were set to the experimentally measured average values. Force constants for the organic linkers were adopted from the Amber force field.[18] The parameters involving the Zn atoms were derived by fitting to experimental lattice constants. In 2013, the same group published a refined version of their original FF in order to be able to model the sorption-induced structural transition by hybrid MC/MD simulations.[19] The crucial torsions around the Zn atom were fitted to a single experimental N_2 isotherm. In a parallel effort, several FFs for ZIF-8 were developed by Demontis et al. In 2011, they published partial charges for several ZIF systems derived from cluster calculation and periodic DFT calculations.[20] In 2012, the first FF based on these partial charges was published,[21] which is again based on Amber. Missing parameters for the organic linker were obtained via the `parmcal` software,[22] which calculates bond-length and bond-angle parameters based on empirical rules. The parameters necessary to describe the tetrahedral ZnN_4 were taken from cluster-based quantum-chemical calculations[23−25] performed in order to be able to describe Zn containing biomolecules by Amber. In 2014, this group published a new FF based on a force-matching parametrization scheme.[26] Zheng et al. published an additional FF for ZIF-8 in 2013.[27] They added an artificial long-range bond between the carbon atoms in neighboring imidazolate linker in a 6-ring window in order to be able to describe the "swing effect" in the correct way. Wu et al. also developed a force field for ZIF-8, again based on Amber, UFF, and experimental data. The parameters for the tetrahedral ZnN_4 were adopted from the already mentioned force field by Jiang et al. from 2013.[19] In 2018, Verploegh et al. published a study on the molecular diffusion in binary mixed linker ZIFs using a flexible FF called intraZIF-FF, whose parametrization methodology has not been published to date.[28]

It is thus clear that the majority of these force fields have been parametrized in a manually involved and ad hoc manner, often mixing different sources, ranging from different other force fields to experimental and theoretical reference data, which makes it difficult to transfer these parametrization methodologies to new systems for which less reference data is available (e.g. in high-throughput screening of hypothetical systems).

On the contrary, we have developed over the years a consistent, transferable and automatic parametrization strategy with the intention to trade transferability for accuracy. It is

based on a machine learning approach using evolutionary algorithms to derive all bonded parameters at once, relying only on a small set of first-principles reference data, namely, ab initio calculated structure and Hessian H.[29] This methodology is called MOF-FF[30] and was recently extended to parametrize also coarse-grained FFs for MOFs.[31−33]

In the meantime, other groups have published related approaches to derive FFs for MOFs in a consistent fashion,[34,35] including the Quick-FF methodology, which uses a different approach to derive the parameters from the same type of reference data as in MOF-FF.[36] MOF-FF and Quick-FF force fields are available for a variety of different MOF families. Yet, force fields for the important family of ZIFs are still missing. A reason for this could be that until recently both methodologies were not capable of treating periodic reference data, which is almost necessary for deriving a ZIF force field from scratch since it is very difficult to construct a representative cluster model for ZIFs. Rana and co-workers showed, for example, that one needs a cluster with a size of 400 to 500 atoms to converge partial charges on the core atoms of the cluster, because a ZIF is made up by charged fragments and charge neutrality is only achieved in the periodic system.[20] Recently, Vanduyfhuys et al. extended the Quick-FF methodology in a way that also periodic reference data can be treated.[37]

In this study, we improved the MOF-FF methodology in several aspects to be able to parametrize force fields in respect to periodic reference data. We demonstrate its capabilities by parametrizing force fields for ZIFs of varying topology and chemical composition (ZIF-8, ZIF-8(H), ZIF-8(Cl) and ZIF-8(Br)). We thus implemented the possibility of handling periodic reference data and introduced a more efficient optimizer. The obtained FFs were then validated in great detail against experimental and ab initio calculated data. We focused especially on the question how well the ZIF flexibility (swing effect) is reproduced by our FFs, as it is crucial to their description and rather difficult to capture. Furthermore, we questioned the transferability of our FFs by applying them to polymorphs for which they were not parametrized.

2. METHODS

The basic idea behind the MOF-FF parametrization procedure is visualized in Figure 1. The reference information, that is, the DFT-optimized structure and the curvature information represented in the matrix of the second derivatives of the
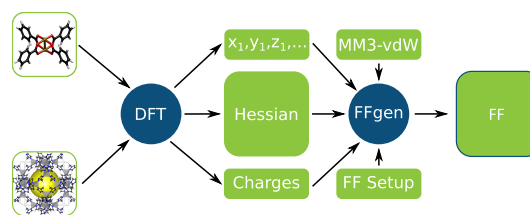
Figure 1. General scheme of the MOF-FF parametrization methodology. First, the reference information (optimized structure, Hessian H, and atomic charges) is calculated by DFT for a given reference system, which could be either a representative cluster or a periodic system. This information is then used together with the corresponding van der Waals parameters—taken from the MM3 force field—as input for FFgen, which tries to identify the best matching bonded parameters for the actual FF setup with respect to the provided reference information.

energy in respect to the coordinates $\vec{\nabla}^2 E$ called Hessian H, are calculated for a given reference system and serve as input for the FFgen code (written in Python). The code is then used to find the best matching bonded parameter set P of the predefined force field energy expression in respect to the provided reference information for a given set of a priori defined van der Waals (vdW) potentials and charges. Whereas charges were calculated by a fit to the electrostatic potential of the optimized reference structure, vdW parameters were taken from the well-known MM3 force field[38,39] and used within the dispersion damped Buckingham potential, as implemented in MOF-FF.[30]

During the parametrization process, a so-called objective function Z is used to measure how well a set of parameters P reproduces the reference data. This objective function is then minimized by a suitable numerical optimizer. An optimization cycle consists of the following three steps: first, the atomic positions of the reference system are relaxed. Second, the Hessian H is calculated by a double sided finite difference approach. Third, the objective function Z is evaluated. For this purpose geometry and Hessian are projected from Cartesian coordinates to redundant internal coordinates (RICs). The RICs comprise more than the usual $3N - 6$ coordinates and are made up by all bonds (str), angles (ibe), dihedrals (tor) and improper dihedrals (obe) of the system, which are also used to calculate the bonded energy of the system in the FF. The reformulated objective function Z_{MOF-FF} is displayed below.

$$Z_{\text{MOF-FF}}(P) = Z_{\text{str}}(P) + Z_{\text{ibe}}(P) + Z_{\text{obe}}(P) + Z_{\text{tor}}(P) + Z_{\text{hes}}(P) \tag{1}$$

It is composed of four parts, measuring the difference for a specific RIC type between reference and force field, and a fifth contribution determined by the difference in the diagonal terms of the projected Hessians. Every term is formulated as weighted mean square deviation between FF and reference as shown for the example of $Z_{\text{str}}(P)$ below:

$$Z_{\text{str}}(P) = \frac{w_{\text{str}}}{M_{\text{str}}} \sum_{i=1}^{N_{\text{str}}} \omega_i (r_i(P) - r_i^{\text{ref}})^2 \tag{2}$$

where the sum runs over all bonds r_i in the system and the individual weights ω_i per redundant internal coordinate q are assigned on the basis of the atomtypes in the system. If a RIC i, defined by its atom types, occurs n_i times in the system, it gets a weight of $\omega_i = n_i^{-1}$. The condition, therefore, is such that the parameters belonging to the FF term describing the RIC of interest are in the set of variable parameters P. Furthermore, since $M_{\text{str}} = \sum_{i=1}^{N_{\text{str}}} \omega_i$, all single contributions to $Z_{\text{MOF-FF}}$ are weighted in the same manner. Of course, this is somehow arbitrary, since different RIC types have different units. Bond lengths are compared in Å, angles in rad, and force constants in mdyn/Å (bonds) or mdynÅ/rad^2 (angles). With this choice all contributions to $Z_{\text{MOF-FF}}$ are roughly in the same order of magnitude. The weight w_{str} can be used to increase the importance of Z_{str} to the overall objective function $Z_{\text{MOF-FF}}$. In addition, one could include the off-diagonal elements of the Hessian in the objective function if also the corresponding cross terms are fitted.

The advantage of this reformulated objective function is a proper weighting, since in the original formulation the RICs were weighted all equally with the consequence that RICs get

a higher weight in the overall objective function when they occur more often in the system.

2.1. Fitting to Periodic Reference Data. Besides the reformulated objective function, the first main innovation affects the input required by FFgen: To parametrize FFs for ZIFs and other materials, in which it is not trivial to derive a representative zero-dimenesional cluster, we extended the parametrization strategy to use reference data that is periodic in one, two or three dimensions.

Technically, the support for periodic reference data was implemented by including periodic boundary conditions (PBCs) in the calculation of Wilson's B-matrix, by augmenting the objective function with a stress-dependent term and by coupling FFgen with the well-known LAMMPS molecular dynamics simulator.[40]

Wilson's B-matrix is needed to for the projection into redundant internal coordinates and is defined in eq 3, where the q_i are the internal coordinates and the x_j are the Cartesian ones. The matrix measures how an internal coordinates q_i changes when a Cartesian coordinate x_j has changed. In the course of this study, we have implemented that PBCs are considered when B is calculated.

$$B_{ij} = \frac{\partial q_i}{\partial x_j} \tag{3}$$

As already mentioned, only the atomic positions are relaxed in every optimization cycle, whereas the lattice is kept fixed. To ensure that the force field also describes the lattice dimensions in the correct way, we introduced an additional term Z_{lattice} which depends on the stress tensor S and penalizes parameter sets P, which cause a large stress tensor for the optimized geometry. Z_{lattice} is defined as follows:

$$Z_{\text{lattice}} = \left(\frac{1}{9} \sum (C^{-1} \cdot (S \cdot V))^2 \right)^2 \tag{4}$$

where V is the cell volume, and C is the cell tensor. This additional term was then weighted by a factor of 0.1 and added to $Z_{\text{MOF-FF}}$. Another option to include the cell shape in the objective function would be to run, in addition to the atomic relaxation, an additional lattice optimization; however, we did not follow this approach because of its higher computational cost.

To handle periodic input data, it is necessary to use a molecular mechanics back-end, which is able to handle relatively small unit cells and is therefore not subject to the minimum image convention. For this reason, the MOF-FF total energy expression was implemented in LAMMPS and coupled to FFgen. An additional advantage of this coupling is the ability to set up the total energy expression using any potential implemented in LAMMPS. This makes FFgen a versatile tool for the parametrization of classical FFs in general and not only in the MOF-FF formulation.

A New Optimizer: CMA-ES. The second main innovation affects the algorithm, which is used to optimize the objective function. Optimization of the objective function is not trivial because the search landscape is relatively bumpy with a lot of local minima. For this purpose, we rely on a stochastic zero-order optimizer which is able to escape from a local minimum. Such optimizers are also often referred to as *black-box optimizers* because they do not need any further information besides the actual value of the objective function at a given search point. In the original MOF-FF parametrization, the
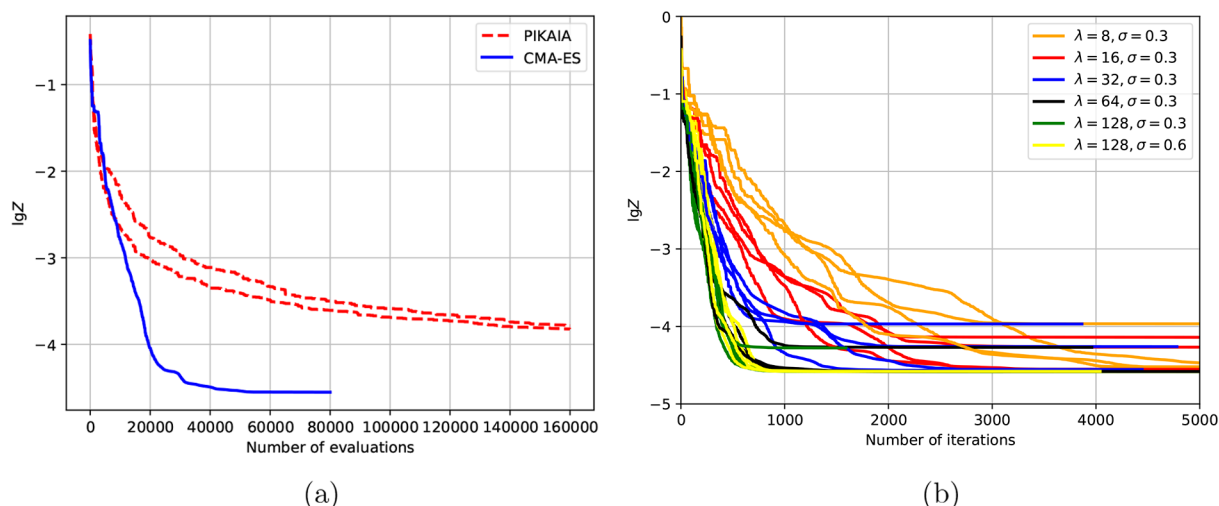
Figure 2. Logarithmic convergence behavior of (a) the originally employed PIKAIA genetic algorithm vs CMA-ES for a parametrization run of ZIF-8(Br) and (b) for several parametrization runs of ZIF-8(Br) using CMA-ES but different population sizes λ and initial step sizes σ.

PIKAIA optimizer was used,[41] which is a genetic algorithm specifically designed for use on continuous variables. Generally, genetic algorithms are employed for optimization on discrete variables, thus in order to represent the continuous variables in a genome of discrete numbers, one has to predefine for every parameter p_i a range consisting of an upper p_i^{max} and a lower bound p_i^{min} so that it holds $p_i^{min} \le p_i \le p_i^{max}$. One limitation of this approach is thus that it is necessary to define these ranges a priori. If the solution is outside of the range, it must be readjusted manually.

Furthermore, the periodic reference systems used in this study are substantially larger than the cluster models employed before. The primitive cell of ZIF-8 consists of 138 atoms and is more than a factor of 2 larger than e.g. a benzoate paddle-wheel unit. We thus needed to change the optimizer to reduce the computational cost of the parametrization process. We implemented in our FFgen code an algorithm called Covariance Matrix Adaption Evolution Strategy (CMA-ES), which was developed by Hansen for optimization problems on continuous variables.[42,43] CMA-ES has previously been applied for force field development, namely, for deriving coarse grained FFs for MOFs[33] and recently for the parametrization of ReaxFF.[44]

In a nutshell, CMA-ES iteratively adopts a multivariate normal distribution (starting from an isotropic normal distribution with an initial width σ) in the parameter space to find a distribution whose random samples minimize the objective function. Thus, the individuals of a generation of size λ are sampled from a multivariate normal distribution where recombination is done by selecting a new mean for the distribution. During the optimization process, the covariance matrix is updated in order to optimize the shape of the multivariate normal distribution with respect to the search landscape defined by the objective function. This amounts to learning a second order model of the objective function similar to the approximation of the inverse Hessian in quasi-Newton optimization methods, which are known for their quadratic convergence near the optimum.[45] A more elaborate description of the optimizer can be found in the Supporting Information. CMA-ES is implemented in FFgen using the ask-and-tell interface of the pycma library.[46] We accelerated the

parametrization process by distributing the evaluation of the fitness function over parallel processes.

Using CMA-ES instead of PIKAIA leads to a substantially faster convergence. To validate this claim we fitted a force field for ZIF-8(Br), using the same setup as described in Section 4.1.3, with both optimizers. The convergence behavior is visualized in a logarithmic scale in Figure 2a. One evaluation of the objective function takes around 2 s on a single core of a current desktop GNU/LINUX workstation.

A further advantage of CMA-ES is that it is not necessary to define a priori any ranges for the parameters as needed in PIKAIA. But defining ranges can be very helpful for the following reasons: at the startup of the algorithm an isotropic normal distribution with a predefined stepsize σ is initialized. Since the parameters differ by their units, they have different orders of magnitude. For this reason, we define every parameter in reduced parameter units by the help of an upper and a lower bound:

$$\bar{p}_i = \frac{p_i}{p_i^{max} - p_i^{min}} \tag{5}$$

However, in contrast to PIKAIA, the ranges are in general not hard constraints, so the parameter is allowed to escape them. Hard ranges are only applied to prevent unphysical parameters like negative bond lengths, bond angles, or force constants.

The optimizer is started from an educated guess for the parameters and their appropriate ranges. For bond lengths r and bond angles θ, it is started from the geometrically measured values of the reference system. Upper and lower bounds were by default set to ± 10 from the geometrically measured average value. For bond and angle force constants, initial ranges are usually defined as 0 mdyn Å^{-1} $\le p_i \le$ 8 mdyn Å^{-1} and 0 mdynÅ/rad^2 $\le p_i \le$ 2 mdyn Å/rad^2. For dihedral potentials, 0 kcal mol^{-1} $\le p_i \le$ 20 kcal mol^{-1} was used as range for the barrier, and for out-of-plane potentials, 0 mdynÅ/rad^2 $\le p_i \le$ 1 mdynÅ/rad^2 was the default. The initial value was set to $\bar{p}_i = 0.5$.

3. COMPUTATIONAL DETAILS

3.1. Obtaining the Reference Information. The reference information needed for the FF optimization was

obtained with periodic DFT calculations using the QUICK-STEP/CP2K package.[47] QUICKSTEP/CP2K is based on a hybrid Gaussian plane-wave approach combining a Gaussian basis for the wave functions with an auxiliary plane wave basis set for the representation of the density.

We found that it is crucial to use a high plane-wave cutoff E_{cut} to obtain accurate Hessians, since in the QUICKSTEP module, the computation of Coulomb and exchange-correlation energies is performed on a real space grid. This representation breaks the translational invariance of the system, which can lead to spurious forces on the atoms (egg box effect), which can have a large influence on the Hessian calculated by a finite difference approach based on the atomic forces.[48]

The gradient-corrected PBE functional[49] was used with an empirical correction for the dispersive interactions using the "D3" method by Grimme et al.[50] Double-ζ valence polarized Gaussian basis sets were employed for all atoms. For C, H, and N, basis sets optimized for usage with the PBE functional were employed, whereas on Zn, Cl, and Br, basis sets optimized for molecules (MOLOPT) were employed. The interaction between ions and valence electrons was represented by Goedecker−Teter−Hutter (GTH) type pseudopotentials.[51−53] Given the systems' size, the Brillouin zone was sampled at the Γ point only.

In order to obtain accurate reference data, strict convergence criteria had to be chosen both for the SCF and for the geometry optimizations. For the SCF a convergence criterion 10^{-10} Hartree was applied, whereas for the optimizations the RMS force has to be lower than 10^{-7} Hartree/bohr. Wherever possible, primitive cells were used for all DFT calculations. The reference data generation can be divided into four steps:

1. Atomic coordinates and the lattice dimensions were optimized using a plane-wave cutoff for the density E_{cut} of 600 Ry (systems without Cl or Br) and 700 Ry (systems with Cl or Br) together with a relative cutoff E_{cut}^{rel} of 40.Ry

2. Afterward only the atomic coordinates were reoptimized using a cutoff E_{cut} of 2500 Ry together with a relative cutoff of E_{cut}^{rel} of 100 Ry. These cutoffs were used for all subsequent calculations.

3. The Hessian of the optimized structure was calculated by the help of a double-sided finite difference scheme using a distortion of at least 0.001 bohr.

4. Charges were calculated by the REPEAT method[54] using its implementation in CP2K. For this purpose, two type of constraints were employed: The total charge of the system has to be zero, and atoms with equal atom types get the same charges.

3.2. Ab Initio Molecular Dynamics Simulations. We performed ab initio molecular dynamics simulations (AIMD) of the ZIF-8 isomorphs with Born−Oppenheimer dynamics using DFT for the calculation of the energy and the atomic forces using the QUICKSTEP/CP2K package. We used the same functional, dispersion correction, and basis sets as for the static calculations described in Section 3.1. The cutoff for the density plane-wave basis set was set to 600 Ry.

We performed all AIMD simulations using periodic boundary conditions on a single crystallographic unit cell of the material ($a_{ZIF-8(H)}$ = 16.808 Å, a_{ZIF-8} = 16.991 Å, $a_{ZIF-8(Br)}$ = 16.985 Å, $a_{ZIF-8(Cl)}$ = 16.998 Å). We used deuterated hydrogen

atoms to allow for a larger time step (1 fs) in the integration of the equations of motion. Simulations were run in the canonical ensemble (N, V, T) using a CSVR[55] thermostat with a time constant of 1 ps to control the temperature. The total simulation time was between 30 and 40 ps depending on the isomorph.

For comparison, we also used data based on BLYP[56,57] AIMD simulations published in a previous study. Further details on these simulations can be found in the original publication.[10]

3.3. Classical Molecular Dynamics Simulations. Classical molecular dynamics simulations were performed using our in-house developed PYDLPOLY code on $2 \times 2 \times 2$ crystallographic unit cells of the material, employing the same lattice constants as used for the AIMD simulations. Simulations were run in the canonical ensemble (N, V, T) using a Berendsen thermostat for equilibration runs of 0.1 and a Nosé−Hoover thermostat for sampling runs of 1 ns. Thermostat relaxation times were set to 0.2 and 2.0 ps.

3.4. Calculation of Elastic Constants. Elastic constants C_{ij}, which are the coefficients of the second-order elastic tensor C, were computed by using the numerical first derivative of the cell gradients corresponding to the each elastic coefficient C_{ij}. For this purpose the optimized structure was deformed in each possible direction, applying both negative and positive strain (corresponding to compression and tension), and for each deformation the atomic coordinates were energy-minimized. For deformations along the normal coordinates, strains of −1.0% to 1.0% in steps of 0.5% were applied, whereas for shear deformations, strains were from −4.0% to 4.0% in steps of 2.0%. The PYMATGEN package was used to deform the structures and to perform the final analysis,[58] using the crystallographic unit cell as a reference configuration. Elastic constants at the ab initio level of theory were computed using the QUICKSTEP/CP2K package employing the same setup as used for the production of the reference data. Elastic constants at the FF level were computed by using PYDLPOLY and a $2 \times 2 \times 2$ supercell.

4. RESULTS AND DISCUSSION

4.1. FF Parameterization. *4.1.1. Systems of Interest.* We focused in this study on the development of four different FFs for ZIF-8, ZIF-8(H), ZIF-8(Br), and ZIF-8(Cl). All are composed of zinc and differently functionalized imidazolate linkers, and they form 3D crystalline networks with the **sod** topology (chemical composition and atom types shown in Figure 3).

Furthermore, we calculated also the reference data for six other polymorphs with the ZIF-8(H) composition, which we used to probe into the transferability of the FFs between different topologies. Crystallographic and chemical information about the investigated systems are listed altogether in Table 1.

4.1.2. Partial Charges. The atomic partial charges obtained for ZIF-8, listed in Table 2, are in good agreement with those published by Rana et al.[20] These authors computed both single-point charges for a high-symmetry relaxed structure of ZIF-8 and charges as average over several snapshots obtained from ab initio MD simulations in the Born−Oppenheimer scheme and in the Car−Parrinello scheme. From the difference between them, they concluded that single-point charges are in agreement with the average value during the time evolution of the system and are thus sufficient. Since they
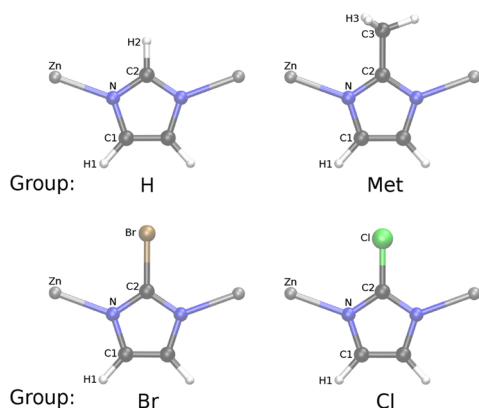
Figure 3. Chemical systems investigated in this study, showing the atom typing used throughout the text.

Table 1. Summary of the Systems Investigated in This Study

	space group	Bravais lattice	net topology	functional group
ZIF-1	$P2_1/c$	mono	crb	H
ZIF-4	$Pbca$	ortho	cag	H
ZIF-6	$I4_1/amd$	tetra	gls	H
ZIF-8(H)	$I\bar{4}3m$	cubic	sod	H
coi	$I4_1$	tetra	coi	H
nog	$P2_1c$	mono	nog	H
zni	$I4_1cd$	tetra	zni	H
ZIF-8(Br)	$I\bar{4}3m$	cubic	sod	Br
ZIF-8(Cl)	$I\bar{4}3m$	cubic	sod	Cl
ZIF-8	$I\bar{4}3m$	cubic	sod	Met

did not calculate charges for ZIF-8(H), ZIF-8(Cl), and ZIF-8(Br), we demonstrate by this comparison the validity of the methodology to derive charges for our FF and used it also for ZIF-8(H), ZIF-8(Cl), and ZIF-8(Br).

For the seven hydrogen-substituted ZIF polymorphs, the charges are shown in Table S1. Depending on the topology, the charges on the Zn range from 0.4645 e to 0.5971 e with a standard deviation of 0.04 e, indicating that the impact of the topology on the charges is relatively minor, compared with the natural methodology-related uncertainty. We thus chose as charges used for our FF a unique set of partial charges for this class of materials, obtained by averaging over the seven structures.

In addition, the charges for the halogen-substituted structures are listed in Table S2. The charges in the Zn atoms for the four chemically distinct species in the **sod** topology differ up to 50% (ZIF-8:0.7290 e, ZIF-8(H): 0.5118 e, ZIF-8(Cl): 0.4986 e, ZIF-8(Br): 0.4714 e). This demonstrates the considerable impact of the substituent on the whole framework and emphasizes the need for distinct parameter sets for every chemically distinct species, especially

in the case of the nonpolarizable MOF-FF where no Coulomb exclusions are applied.

4.1.3. Intramolecular Parameterization. The force field energy expression was set up for the four systems in the way that only diagonal terms were applied, and no cross terms like stretch−bend potentials were used. All dihedral potentials were set up by imposing a multiplicity of two, besides the C2−N−Zn−N and C1−N−Zn−N where a multiplicity of three was used. Because of the disorder of the methyl groups, no dihedral potential was applied for N−C2−C3−H3 dihedral in ZIF-8(H), and the involved parameters were predefined for the actual parametrization. The comparison of the actual dihedral angle values was not included in the objective function (except in the case of ZIF-8, where $w_{tor} = 0.1$ was employed), because the geometry is already imposed by the chosen multiplicity of the potential. Charges were chosen as described above, and MM3 vdW parameters were employed. Equal weights of one were assigned to all different contributions (w_{str}, w_{ibe}, w_{hes}) of the objective function Z.

When using heuristic optimizers like CMA-ES on bumpy search landscapes, it is recommended to run the optimizer several times with increasing population sizes.[59] For this reason, we always started several runs by increasing the populations size λ from the default size ($\lambda = 4 + (3 \ln N_{par}) = 16$) up to 32 individuals per generation. To prove that $\lambda = 32$ is sufficient, we performed additional parametrization runs with population sizes from 8 to 128 individuals for ZIF-8(Br). Furthermore, we conducted additional runs with 128 individuals and a doubled step size $\sigma = 0.6$. The results shown in Figure 2b demonstrate that $\lambda = 32$ is an appropriate population size for our problem. In addition, during our restart strategy we also perturbed the parameter ranges, if we felt that they were too loose or too strict.

4.2. Force Field Validation. *4.2.1. Structural Properties.* As a first validation step, we verified how well the parametrized FFs reproduce the structural properties of the materials, with respect to DFT-optimized structures. Figure 4 shows a comparison between the final bond lengths, bending angles, and dihedral angles obtained at the two levels of theory. In the case of the FFs, we have also relaxed the lattice for this comparison. Note that since no Coulomb exclusion is used in MOF-FF and because of the complex periodic structures, it is not clear beforehand that these structural parameters are always reproduced correctly. Overall agreement is excellent, with the biggest deviations observed for ZIF-8, which is due to the disorder introduced by the methyl groups' free rotation and the fact that no dihedral potential is included for the N−C2−C3−H3 torsion. We also investigated the lattice dimensions at zero Kelvin (full cell energy optimization) in comparison to the DFT results; see Table 3. The lattice dimensions of the structures which served as reference systems for the parametrization coincide almost perfectly. The biggest difference of 0.05 Å arises for ZIF-8, which is again due to the

Table 2. REPEAT Charges (Units in Partial Electron Charges) for ZIF-8 Computed by Us in Respect to the Optimized Structure in Comparison to Those Published by Rana et al. Based on Snapshots Extracted from BOMD and CPMD Simulations[20]

	Zn	N	C1	C2	C3	H1	H3
SP	0.7290	−0.3417	−0.1923	0.4937	−0.5276	0.162	0.1373
BOMD	0.7362	−0.3008	−0.1924	0.4339	−0.6042	0.1585	0.1572
CPMD	0.6894	−0.2800	−0.1910	0.418	−0.5726	0.1536	0.1481
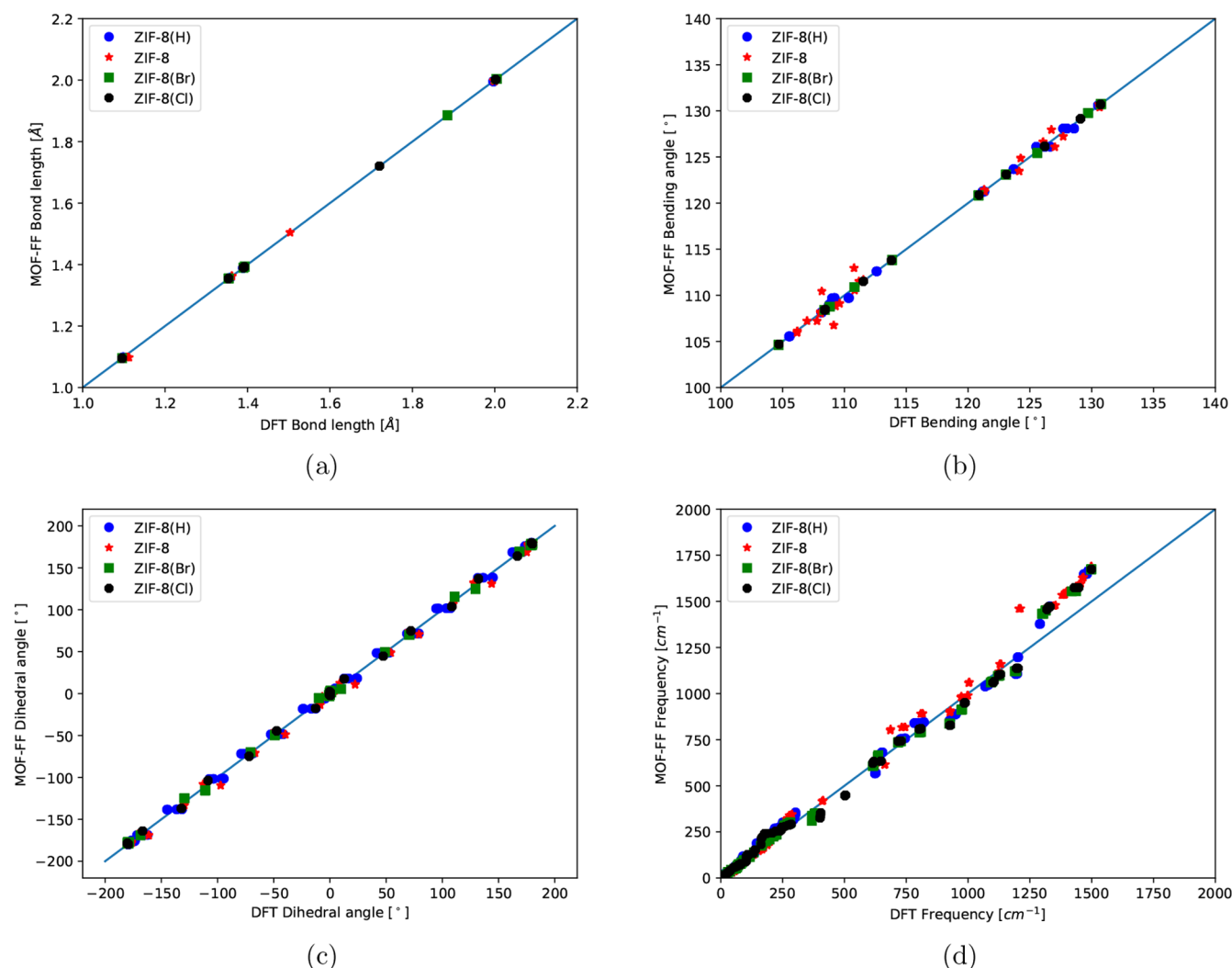
Figure 4. Scatter plots visualizing the performance of our FFs with respect to the ab initio reference data. (a) Comparison of bond lengths. (b) Comparison of bond angles. (c) Comparison of dihedral angles. (d) Comparison of vibrational normal modes.

disorder introduced by the methyl groups. The MOF-FF parametrization methodology relies on a single-structure fit, which works best as long as structures are highly ordered and only one isomeric form exists.

4.2.2. Deformations: Vibrations and Elasticity. Next we checked the accuracy of the FFs in representing deformations from the relaxed structures, comparing normal-mode frequencies and elastic constants, which are directly linked to the second derivative of the energy in respect to the atomic coordinates and unit cell parameters, respectively.

Figure 4d shows the comparison of the FF normal modes against DFT data. The agreement is good, in particular for the low-frequency vibrations modes. Those modes are maximally delocalized and are mainly responsible for the lattice vibrations and flexibility of the framework, and consequently, they are crucial to reproduce correctly. The modes between 500 and 2000 cm^{-1} are more localized and involve especially distortions of the aromatic imidazolate rings. A possibility of achieving a better accuracy in this region in the future could be the incorporation of cross-terms into the FF.

Elastic constants calculated by different DFT methods— some published in the literature, and some computed as part of this work—are compared to those obtained by our FFs in

Table 4. Zheng et al. predicted recently the elastic constants of differently functionalized ZIFs in the **sod** topology. They found that electron-withdrawing groups improve the mechanical stability of the materials (ZIF-8(H) < ZIF-8(Cl) < ZIF-8(Br)).[62] Although the absolute numbers of our DFT calculations differ up to a few GPa this trend is also reproduced by our calculations. Furthermore, this trend is even reproduced in our force field calculations. The only exception is C_{44}, but already the differences from the reference calculations are here very subtle in comparison to those published in the literature. In general, our FF systematically overestimates C_{11} and C_{12}, whereas it underestimates C_{44}. To improve here, one could either incorporate cross-terms or one could adjust the anharmonicities of the bonded potentials in order to tune the curvature of the effective potential.

4.2.3. Molecular Mechanism of the Swing Effect. The flexibility in ZIF-8 analogues is governed by intraframework dynamics and involves, as detailed in the introduction, the so-called swing effect of the imidazolate linkers that allows molecules larger than its window size to diffuse into the framework. Coudert investigated this effect in detail by ab initio MD simulations.[10] The swinging motion of the imidazolate linkers was characterized by the dihedral angle ϕ

Table 3. Lattice Dimensions for the Investigated ZIF Systems Computed by the FFs and Different DFT Methods

	a [Å]	b [Å]	c [Å]	α [deg]	β [deg]	γ [deg]
ZIF-1 cp2k	9.94	14.92	16.45	90.00	118.51	90.00
ZIF-1 FF	10.09	14.55	15.91	90.00	117.00	90.00
ZIF-4 cp2k	14.73	18.30	15.26	90.00	90.00	90.00
ZIF-4[60]	15.58	18.54	15.84	90.00	90.00	90.00
ZIF-4 exp[5]	15.40	18.43	15.31	90.00	90.00	90.00
ZIF-4 FF	14.97	17.67	14.16	90.00	90.00	97.61
ZIF-6 cp2k	19.37	19.37	19.60	90.00	90.00	90.00
ZIF-6 exp[5]	18.52	18.52	20.25	90.00	90.00	90.00
ZIF-6 FF	19.23	19.23	19.80	90.00	90.00	90.00
ZIF-8(H) cp2k	16.97	16.97	16.97	90.00	90.00	90.00
ZIF-8(H)[10]	17.01	17.01	17.01	90.00	90.00	90.00
ZIF-8(H) FF	16.97	16.97	16.97	90.00	90.00	90.00
coi cp2k	17.22	17.22	17.22	98.58	98.58	134.83
coi FF	17.23	17.23	17.22	98.63	98.63	134.34
nog cp2k	24.47	9.60	34.58	90.00	132.19	90.00
nog FF	24.68	9.64	35.03	90.00	134.67	90.00
zni cp2k	23.35	23.35	12.56	90.00	90.00	90.00
zni[60]	23.76	23.76	12.50	90.00	90.00	90.00
zni exp[61]	23.50	23.50	12.46	90.00	90.00	90.00
zni FF	23.23	23.23	12.79	90.00	90.00	90.00
ZIF-8 cp2k	17.03	17.03	17.03	90.00	90.00	90.00
ZIF-8[10]	16.86	16.86	16.86	90.00	90.00	90.00
ZIF-8 exp[5]	16.99	16.99	16.99	90.00	90.00	90.00
ZIF-8 FF	17.08	17.08	17.08	90.00	90.00	90.00
ZIF-8(Br) cp2k	17.25	17.25	17.25	90.00	90.00	90.00
ZIF-8(Br) FF	17.25	17.25	17.25	90.00	90.00	90.00
ZIF-8(Cl) cp2k	17.20	17.20	17.20	90.00	90.00	90.00
ZIF-8(Cl) FF	17.21	17.21	17.21	90.00	90.00	90.00

Table 4. Elastic Constants of ZIF-8, ZIF-8(H), ZIF-8(Br), and ZIF-8(Cl) Computed by the FFs and Different DFT Methods

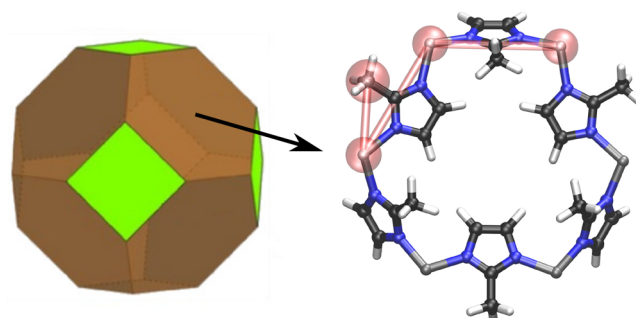|	C_{11} [GPa]	C_{12} [GPa]	C_{44} [GPa]
ZIF-8 FF	8.54	6.55	0.62
ZIF-8[63]	11.04	8.32	0.94
ZIF-8(H) FF	6.65	4.95	1.12
ZIF-8(H) cp2k	5.39	4.51	0.32
ZIF-8(H)[62]	8.95	7.59	2.36
ZIF-8(Cl) FF	9.92	7.84	0.46
ZIF-8(Cl) cp2k	9.23	7.35	0.86
ZIF-8(Cl)[62]	12.30	9.98	3.58
ZIF-8(Br) FF	10.41	8.65	0.19
ZIF-8(Br) cp2k	10.33	8.31	0.88
ZIF-8(Br)[62]	15.92	11.57	6.56

Figure 5. Sodalite topology **sod** of ZIF-8 and view of the 6-ring window of ZIF-8, with the swing dihedral angle ϕ marked in light red. The reference angle of 0° is the plane of the 6-ring.

$Zn_3-Zn_2-Zn_1-CH_3$ of the imidazolate around the Zn_1-Zn_2 axis, where the "reference" of 0° is the 6-ring of Zn (i.e., the window connection the cages) as shown in Figure 5.

We used our force fields to run classical MD simulations in the (N, V, T) ensemble using the same lattice constants as in the corresponding AIMD for the different functionalizations to compare with the DFT results. Originally only ZIF-8 and ZIF-8(H) were investigated using the BLYP functional.[56,57] We performed further AIMD simulations, in the course of the
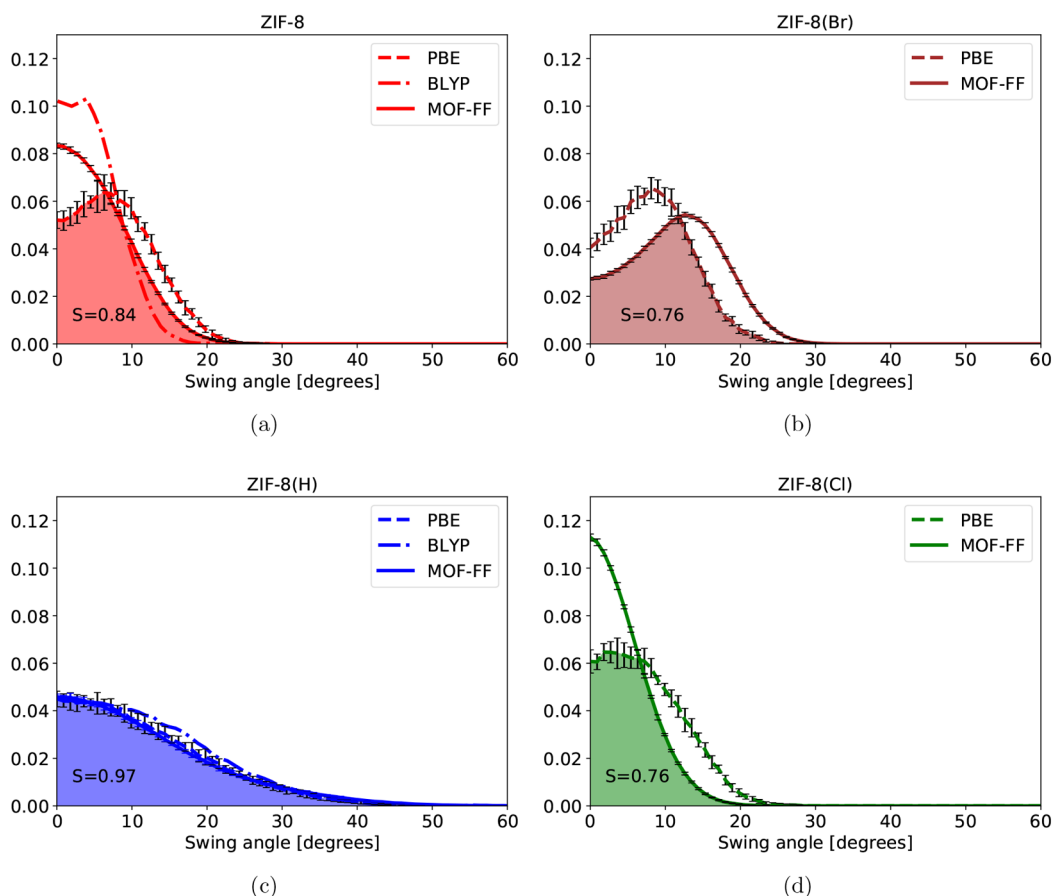
Figure 6. Histograms of the swing angle of the imidazolate linkers, for ZIF-8 (a), ZIF-8(Br) (b), ZIF-8(H) (c), and(ZIF-8(Cl) (d) computed at different levels of theory. For every chemically distinct system, the overlap between the FF and our reference DFT method is plotted together with the histogram intersection S, giving the cumulative overlap. Uncertainties on the histograms were determined by dividing each trajectory into 10 evenly spaced and randomly arranged subtrajectories, and calculating the histogram for each of them. We plotted always $\pm 2\sigma$ as error.

present work and the work by Chaiplas et al.,[64] for ZIF-8, ZIF-8(H), ZIF-8(Br), and ZIF-8(Cl) using the PBE functional.

Histograms of the swinging angle ϕ for the four different systems are shown in Figure 6. For ZIF-8, data from both PBE and BLYP is available (see Figure 6a). From the difference between them, one can estimate the errors made by different DFT exchange−correlation functionals which is an important measure for the accuracy of FFs. As one can see, the differences are quite substantial, the histogram calculated with PBE has a larger spread, the "thermal" swing motion goes up to 20°, whereas in the case of BLYP, it is only 15°. The histogram predicted by MOF-FF lies in between the two curves predicted by the two functionals having a cumulative overlap to the PBE functional of $S = 0.84$.

For ZIF-8(H) again data from both functionals is available (see Figure 6c). Here the PBE and BLYP curves are more similar as in the case of ZIF-8. As already predicted by Coudert ZIF-8(H) exhibits a swing motion with much larger amplitude than ZIF-8. This effect is nicely resembled by our force field, resulting in a cumulative overlap S of 0.97. The thermal swing motion goes all the way up to 35° (instead of 20° for ZIF-8).

For the halogenated species (ZIF-8(Cl) and ZIF-8(Br)) the agreement between FF and DFT calculated data is less good than for ZIF-8 and ZIF-8(H), resulting for both systems in a cumulative overlap of $S = 0.76$. For ZIF-8(Br) the general

shape of the curve is reproduced well but it is stretched along the x-axis toward higher swing angles by 5° (see Figure 6b). In case of ZIF-8(Cl), the FF predicted curve is compressed to lower swing angles by 5° degrees (see Figure 6d). We emphasize, however, that these differences are of the same order of magnitude as the difference between the curves for ZIF-8 predicted at the DFT level of theory by the different exchange−correlation functionals.

4.2.4. Transferability and Overfitting. In general, the MOF-FF strategy of parametrizing a FF is to use nonperiodic reference information if possible. This has the advantage of fitting in respect to sterically relaxed building blocks, which should increase the transferability of the FFs. For example, our Copper paddle-wheel (PW) force field is not parametrized in respect to HKUST-1, but in respect to the benzoate saturated PW in vacuum. This allows us to investigate PWs in different strained environments like MOF-14 and HKUST-1 (i.e., in the **tbo** and **pto** topology).[65] However, in the current work, we chose a different strategy, since we fitted directly to the strained periodic structure. In the following, the transferability of the FF to other topologies and the amount of overfitting is assessed.

We thus optimized the structure of six ZIF-8(H) polymorphs and compared the energies to DFT results, obtained in this work as well as previously by Baburin et al.[66] (who did, however, not include any dispersion corrections). Is
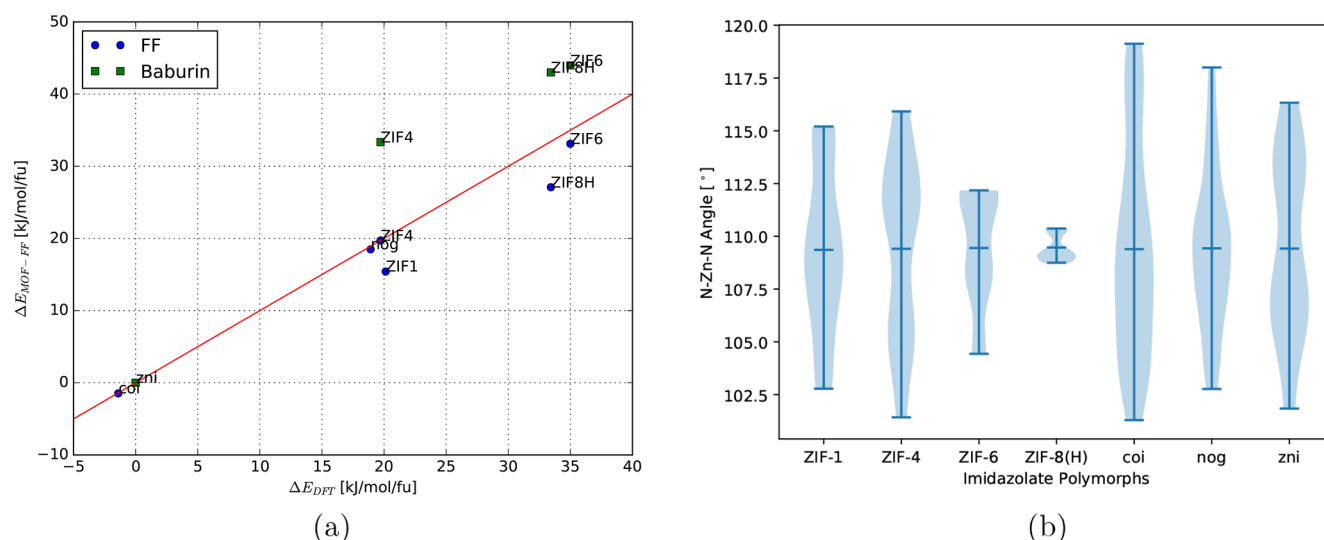
Figure 7. (a) Scatter plot of the total energies of the 7 ZIF-8(H) polymorphs computed by the FF and two different DFT methods, namely, by Baburin et al.[66] and us as described in Section 3.1. (b) Violin plot of the N−Zn−N angle distributions in the seven ZIF-8(H) polymorphs, based on the DFT optimized structures. Minimal and maximal values are shown together with the mean of the distributions.

it possible to reproduce the relative stabilities of the isomorphs and predict the correct energetic ordering? The results are shown in Figure 7a. DFT predicts the following energetic ordering: coi < zni < nog < ZIF-4 < ZIF-1 < ZIF-8(H) < ZIF-6, whereas the FF predicts coi < zni < ZIF-1 < nog < ZIF − 4 < ZIF-8(H) < ZIF-6. Thus, the only difference is that the stability of ZIF-1 is overestimated. The reason for this can be found in the lower symmetry of the other polymorphs compared with ZIF-8(H), which was used as a reference system. Figure 7b shows the distribution of the N−Zn−N angles for the other investigated polymorphs based on the DFT optimized structures. They show substantially larger deviations from the ideal tetrahedron angle as compared to ZIF-8(H). So they are further away from the reference structure, which results in a worse performance. The same behavior can also be observed for the lattice constants of the other polymorphs as shown in Table 3. In comparison to the systems which served as reference information, they show an inferior performance; however, they are still well within the range of lattice constants predicted by different DFT methods. An exception is ZIF-4. The reason for this difference is not only the lower symmetry of the Zn coordination environment but also the existence of several different phases of ZIF-4, which bedevils the situation for a FF fitted in respect to the **sod** topology. Finally, we checked how well our FF describes the elastic tensor of a different polymorph, namely, ZIF-6. DFT predicts the following matrix: $c_{11} = 8.33$ GPa, $c_{12} = 7.58$ GPa, $c_{13} = 10.99$ GPa, $c_{33} = 16.65$ GPa, $c_{44} = 0.67$ GPa, $c_{66} = 0.30$ GPa. The FF predicts: $c_{11} = 6.79$ GPa, $c_{12} = 5.68$ GPa, $c_{13} = 7.62$ GPa, $c_{33} = 12.68$ GPa, $c_{44} = 0.96$ GPa, $c_{66} = 0.55$ GPa. Also, here the same trend is observed, qualitative agreement is achieved, but less quantitative agreement is observed compared with the accuracy on the actual reference system. We note, however, that the predictive power in respect to the other polymorphs could be increased by fitting a FF for each of them, but by this method, one would loose the possibility to compare the relative stabilities between different polymorphs. A solution would be to perform multistructure fits using different polymorphs as reference system at once.

5. CONCLUSIONS

The aim of this study was to exploit the systematic and consistent MOF-FF force field parametrization methodology to arrive at an accurate and efficient potential for a range of ZIFs. By trading transferability for accuracy, we parametrized explicitly for the chemically distinct systems, namely, ZIF-8, ZIF-8(H), ZIF-8(Br), and ZIF-8(Cl), using the **sod** topology as a reference. For this purpose, we needed to improve and extend the original methodology in several aspects. First, we added the possibility to employ also periodic reference systems, which enables us to use our approach also for those systems which can not be easily truncated to a cluster representations (e.g., rod-based MOFs like MIL-53 or MOF-74, or ZIFs in general). Second, we replaced the original genetic-algorithm-based global optimizer by another more efficient evolutionary strategy that is better suited for continuous variables. The CMA-ES converges substantially faster and without constraining to parameter ranges, which is extremely beneficial since the numerical effort for the evaluation of the target function is numerically much more involved in the case of a fit to periodic reference systems like in the case of ZIFs. Furthermore, it also paves the way toward a completely automated black box algorithm for FF parametrization.

As expected, the force fields are able to well reproduce structure and lattice parameters as well as dynamic properties like vibrational normal modes and elastic constants in comparison to available experimental results as well as the computed reference data at the DFT level of theory.

A much more subtle property of ZIFs is their inherent flexibility, namely, the so-called swing effect, which allows molecules larger than the geometric window size to diffuse into the framework by a slight rotation of the imidazolate linkers. The ability of a force field to reproduce this behavior in an accurate way is crucial for its use in simulating guest molecule adsorption or, for example, heat conduction. We find that our force field is able to reproduce this flexibility with an accuracy comparable to ab initio MD simulations.

In order to validate the transferability of the parameter set, the energetic ranking of other ZIF topologies was also tested.

Interestingly, we find that the energetic ordering of the polymorphs ZIF-1, ZIF-4, ZIF-6, **coi**, **nog**, and **zni** computed with the force field fitted to ZIF-8(H) is nicely reproduced as compared to periodic DFT calculations. A further improvement could be achieved by fitting to several reference structures at once to avoid overfitting. Future development efforts will likely aim at an efficient implementation of these multistructure fits.

All in all, this study demonstrates the potential of the here introduced extended MOF-FF parametrization methodology. Based on a single periodic reference structure (geometry and curvature), it is possible to derive an accurate force field in a consistent and systematic way, which can be used to substantially extend length and time scales in MD simulations, within the constraint of no bond breaking, in an accuracy close to periodic DFT.

■ ASSOCIATED CONTENT

ⓢ Supporting Information

The Supporting Information is available free of charge on the ACS Publications website at DOI: 10.1021/acs.jctc.8b01041.

> Detailed information about the MOF-FF energy expression, the projection into redundant internal coordinates, the CMA-ES optimizer, and final parameter sets (PDF)

■ AUTHOR INFORMATION

Corresponding Authors
*E-mail: fx.coudert@chimieparistech.psl.eu.
*E-mail: rochus.schmid@rub.de.

ORCID ⃝
François-Xavier Coudert: 0000-0001-5318-3910
Rochus Schmid: 0000-0002-1933-3644

Notes
The authors declare no competing financial interest.

■ ACKNOWLEDGMENTS

■ REFERENCES

(1) Horike, S.; Shimomura, S.; Kitagawa, S. Soft Porous Crystals. *Nat. Chem.* **2009**, *1*, 695.

(2) Furukawa, H.; Cordova, K. E.; O'Keeffe, M.; Yaghi, O. M. The Chemistry and Appli- cations of Metal-Organic Frameworks. *Science* **2013**, *341*, 1230444.

(3) Ferey, G. Hybrid Porous Solids: Past, Present. *Chem. Soc. Rev.* **2008**, *37*, 191−214.

(4) Farha, O. K.; Hupp, J. T. Rational Design, Synthesis, Purification, and Activation of Metal-Organic Framework Materials. *Acc. Chem. Res.* **2010**, *43*, 1166−1175.

(5) Park, K. S.; Ni, Z.; Côté, A. P.; Choi, J. Y.; Huang, R.; Uribe-Romo, F. J.; Chae, H. K.; O'Keeffe, M.; Yaghi, O. M. Exceptional Chemical and Thermal Stability of Zeolitic Imidazolate Frameworks. *Proc. Natl. Acad. Sci. U. S. A.* **2006**, *103*, 10186−10191.

(6) Schneemann, A.; Bon, V.; Schwedler, I.; Senkovska, I.; Kaskel, S.; Fischer, R. A. Flex- ible Metal−Organic Frameworks. *Chem. Soc. Rev.* **2014**, *43*, 6062.

(7) Bennett, T. D.; Fuchs, A. H.; Cheetham, A. K.; Coudert, F.-X. Flexibility and Disorder in Metal−Organic Frameworks. *Dalton Trans.* **2016**, *45*, 4058−4059.

(8) Wu, X.; Huang, J.; Cai, W.; Jaroniec, M. Force Field for ZIF-8 Flexible Frameworks: Atomistic Simulation of Adsorption, Diffusion of Pure Gases as CH4, H2, CO2 and N2. *RSC Adv.* **2014**, *4*, 16503−16511.

(9) Verploegh, R. J.; Nair, S.; Sholl, D. S. Temperature and Loading-Dependent Diffu- sion of Light Hydrocarbons in ZIF-8 as Predicted Through Fully Flexible Molecular Simulations. *J. Am. Chem. Soc.* **2015**, *137*, 15760−15771.

(10) Coudert, F.-X. Molecular Mechanism of Swing Effect in Zeolitic Imidazolate Framework ZIF-8: Continuous Deformation upon Adsorption. *ChemPhysChem* **2017**, *18*, 2732−2738.

(11) Mortada, B.; Chaplais, G.; Veremeienko, V.; Nouali, H.; Marichal, C.; Patarin, J. Energetic Performances of ZIF-8 Derivatives: Impact of the Substitution (Me, Cl, or Br) on Imidazolate Linker. *J. Phys. Chem. C* **2018**, *122*, 3846−3855.

(12) Heinen, J.; Dubbeldam, D. On Flexible Force Fields for Metal−Organic Frameworks: Recent Developments and Future Prospects. *Wiley Interdisciplinary Reviews: Compu- tational Molecular Science* **2018**, *8*, No. e1363.

(13) Rappe, A. K.; Casewit, C. J.; Colwell, K. S.; Goddard, W. A.; Skiff, W. M. UFF, a Full Periodic Table Force Field for Molecular Mechanics and Molecular Dynamics Simulations. *J. Am. Chem. Soc.* **1992**, *114*, 10024.

(14) Addicoat, M. A.; Vankova, N.; Akter, I. F.; Heine, T. Extension of the Universal Force Field to Metal−Organic Frameworks. *J. Chem. Theory Comput.* **2014**, *10*, 880.

(15) Coupry, D. E.; Addicoat, M. A.; Heine, T. Extension of the Universal Force Field for Metal−Organic Frameworks. *J. Chem. Theory Comput.* **2016**, *12*, 5215−5225.

(16) Boyd, P. G.; Moosavi, S. M.; Witman, M.; Smit, B. Force-Field Prediction of Materials Properties in Metal-Organic Frameworks. *J. Phys. Chem. Lett.* **2017**, *8*, 357−363.

(17) Hu, Z.; Zhang, L.; Jiang, J. Development of a Force Field for Zeolitic Imidazolate Framework-8 with Structural Flexibility. *J. Chem. Phys.* **2012**, *136*, 244703.

(18) Cornell, W. D.; Cieplak, P.; Bayly, C. I.; Gould, I. R.; Merz, K. M.; Ferguson, D. M.; Spellmeyer, D. C.; Fox, T.; Caldwell, J. W.; Kollman, P. A. A Second Generation Force Field for the Simulation of Proteins, Nucleic Acids, and Organic Molecules. *J. Am. Chem. Soc.* **1995**, *117*, 5179−5197.

(19) Zhang, L.; Hu, Z.; Jiang, J. Sorption-Induced Structural Transition of Zeolitic Imidazolate Framework-8: A Hybrid Molecular Simulation Study. *J. Am. Chem. Soc.* **2013**, *135*, 3722−3728.

(20) Rana, M. K.; Pazzona, F. G.; Suffritti, G. B.; Demontis, P.; Masia, M. Estimation of Partial Charges in Small Zeolite Imidazolate Frameworks from Density Functional Theory Calculations. *J. Chem. Theory Comput.* **2011**, *7*, 1575−1582.

(21) Zheng, B.; Sant, M.; Demontis, P.; Suffritti, G. B. Force Field for Molecular Dynamics Computations in Flexible ZIF-8 Framework. *J. Phys. Chem. C* **2012**, *116*, 933−938.

(22) Automatic Atom Type and Bond Type Perception in Molecular Mechanical Calculations. *Journal of Molecular Graphics and Modelling* **2006**, *25*, 247−260.

(23) Hoops, S. C.; Anderson, K. W.; Merz, K. M. Force Field Design for Metalloproteins. *J. Am. Chem. Soc.* **1991**, *113*, 8262−8270.

(24) Lin, F.; Wang, R. Systematic Derivation of AMBER Force Field Parameters Applicable to Zinc-Containing Systems. *J. Chem. Theory Comput.* **2010**, *6*, 1852−1870.

(25) Peters, M. B.; Yang, Y.; Wang, B.; Füsti-Molnár, L.; Weaver, M. N.; Merz, K. M. Structural Survey of Zinc-Containing Proteins and Development of the Zinc AMBER Force Field (ZAFF). *J. Chem. Theory Comput.* **2010**, *6*, 2935−2947.

(26) Gabrieli, A.; Sant, M.; Demontis, P.; Suffritti, G. B. Fast and Efficient Optimization of Molecular Dynamics Force Fields for Microporous Materials: Bonded Interactions via Force Matching. *Microporous Mesoporous Mater.* **2014**, *197*, 339−347.

(27) Zheng, B.; Pan, Y.; Lai, Z.; Huang, K.-W. Molecular Dynamics Simulations on Gate Opening in ZIF-8: Identification of Factors for Ethane and Propane Separation. *Langmuir* **2013**, *29*, 8865−8872.

(28) Verploegh, R. J.; Wu, Y.; Boulfelfel, S. E.; Sholl, D. S. Quantitative Predictions of Molecular Diffusion in Binary Mixed-Linker Zeolitic Imidazolate Frameworks Using Molecular Simulations. *J. Phys. Chem. C* **2018**, *122*, 5627−5638.

(29) Tafipolsky, M.; Schmid, R. Systematic First Principles Parameterization of Force Fields for Metal-Organic Frameworks Using a Genetic Algorithm Approach. *J. Phys. Chem. B* **2009**, *113*, 1341.

(30) Bureekaew, S.; Amirjalayer, S.; Tafipolsky, M.; Spickermann, C.; Roy, T. K.; Schmid, R. MOF-FF − A Flexible First-Principles Derived Force Field for Metal-Organic Frame- works. *Phys. Status Solidi B* **2013**, *250*, 1128−1141.

(31) Dürholt, J. P.; Galvelis, R.; Schmid, R. Coarse Graining of Force Fields for Metal−Organic Frameworks. *Dalton Trans.* **2016**, *45*, 4370−4379.

(32) Dürholt, J. P.; Keupp, J.; Schmid, R. The Impact of Mesopores on the Mechanical Stability of HKUST-1: A Multiscale Investigation. *Eur. J. Inorg. Chem.* **2016**, *2016*, 4517−4523.

(33) Semino, R.; Dürholt, J. P.; Schmid, R.; Maurin, G. Multiscale Modeling of the HKUST-1/Poly(Vinyl Alcohol) Interface: From an Atomistic to a Coarse Graining Approach. *J. Phys. Chem. C* **2017**, *121*, 21491−21496.

(34) Bristow, J. K.; Tiana, D.; Walsh, A. Transferable Force Field for Metal−Organic Frameworks from First-Principles: BTW-FF. *J. Chem. Theory Comput.* **2014**, *10*, 4644.

(35) Bristow, J. K.; Skelton, J. M.; Svane, K. L.; Walsh, A.; Gale, J. D. A General Forcefield for Accurate Phonon Properties of Metal−Organic Frameworks. *Phys. Chem. Chem. Phys.* **2016**, *18*, 29316−29329.

(36) Vanduyfhuys, L.; Vandenbrande, S.; Verstraelen, T.; Schmid, R.; Waroquier, M.; Van Speybroeck, V. QuickFF: A Program for a Quick and Easy Derivation of Force Fields for Metal-organic Frameworks from Ab Initio Input. *J. Comput. Chem.* **2015**, *36*, 1015−1027.

(37) Vanduyfhuys, L.; Vandenbrande, S.; Wieme, J.; Waroquier, M.; Verstraelen, T.; Van Speybroeck, V. Extension of the QuickFF Force Field Protocol for an Improved Accuracy of Structural, Vibrational, Mechanical and Thermal Properties of Metal−Organic Frameworks. *J. Comput. Chem.* **2018**, *39*, 999.

(38) Allinger, N. L.; Yuh, Y. H.; Lii, J. H. Molecular Mechanics. The MM3 Force Field for Hydrocarbons. 1. *J. Am. Chem. Soc.* **1989**, *111*, 8551.

(39) Allinger, N. L.; Zhou, X.; Bergsma, J. Molecular Mechanics Parameters. *J. Mol. Struct.: THEOCHEM* **1994**, *312*, 69−83.

(40) Plimpton, S. Fast Parallel Algorithms for Short-Range Molecular Dynamics. *J. Comput. Phys.* **1995**, *117*, 1−19.

(41) Charbonneau, P. Genetic Algorithms in Astronomy and Astrophysics. *Astrophys. J., Suppl. Ser.* **1995**, *101*, 309.

(42) Hansen, N. *Towards a New Evolutionary Computation*; Studies in Fuzziness and Soft Computing; Springer, Berlin, 2006; pp 75−102.

(43) Hansen, N.; Ostermeier, A. Completely Derandomized Self-Adaptation in Evolution Strategies. *Evol. Comput.* **2001**, *9*, 159−195.

(44) Shchygol, G.; Yakovlev, A.; Trnka, T.; van Duin, A. C. T.; Verstraelen, T. Systematic Comparison of Monte Carlo Annealing and Covariance Matrix Adaptation for the Optimization of ReaxFF Parameters **2018**, *ChemRxiv* e-Print archive. DOI: 10.26434/chemrxiv.6606668.v1.

(45) Minisci, E., Vasile, M., Periaux, J., Gauger, N. R., Giannakoglou, K. C., Quagliarella, D., Eds. *Advances in Evolutionary and Deterministic Methods for Design, Optimization and Control in Engineering and Sciences*; Computational Methods in Applied Sciences; Springer International Publishing, 2019.

(46) Hansen, N. Python Implementation of CMA-ES. CMA-ES, 2019.

(47) VandeVondele, J.; Krack, M.; Mohamed, F.; Parrinello, M.; Chassaing, T.; Hutter, J. Quickstep: Fast and Accurate Density Functional Calculations Using a Mixed Gaussian and Plane Waves Approach. *Comput. Phys. Commun.* **2005**, *167*, 103−128.

(48) Haigis, V.; Belkhodja, Y.; Coudert, F.-X.; Vuilleumier, R.; Boutin, A. Challenges in First-Principles NPT Molecular Dynamics of Soft Porous Crystals: A Case Study on MIL-53(Ga). *J. Chem. Phys.* **2014**, *141*, No. 064703.

(49) Perdew, J. P.; Burke, K.; Ernzerhof, M. Generalized Gradient Approximation Made Simple. *Phys. Rev. Lett.* **1996**, *77*, 3865−3868.

(50) Grimme, S.; Antony, J.; Ehrlich, S.; Krieg, H. A Consistent and Accurate Ab Ini- tio Parametrization of Density Functional Dispersion Correction (DFT-D) for the 94 Elements H-Pu. *J. Chem. Phys.* **2010**, *132*, 154104.

(51) Goedecker, S.; Teter, M.; Hutter, J. Separable Dual-Space Gaussian Pseudopotentials. *Phys. Rev. B: Condens. Matter Mater. Phys.* **1996**, *54*, 1703−1710.

(52) Hartwigsen, C.; Goedecker, S.; Hutter, J. Relativistic Separable Dual-Space Gaussian Pseudopotentials from H to Rn. *Phys. Rev. B: Condens. Matter Mater. Phys.* **1998**, *58*, 3641−3662.

(53) Krack, M. Pseudopotentials for H to Kr Optimized for Gradient-Corrected Exchange- Correlation Functionals. *Theor. Chem. Acc.* **2005**, *114*, 145−152.

(54) Campañá, C.; Mussard, B.; Woo, T. K. Electrostatic Potential Derived Atomic Charges for Periodic Systems Using a Modified Error Functional. *J. Chem. Theory Comput.* **2009**, *5*, 2866−2878.

(55) Bussi, G.; Donadio, D.; Parrinello, M. Canonical sampling through velocity rescaling. *J. Chem. Phys.* **2007**, *126*, No. 014101.

(56) Becke, A. D. Density-Functional Exchange-Energy Approximation with Correct Asymptotic Behavior. *Phys. Rev. A: At., Mol., Opt. Phys.* **1988**, *38*, 3098−3100.

(57) Lee, C.; Yang, W.; Parr, R. G. Development of the Colle-Salvetti Correlation-Energy Formula into a Functional of the Electron Density. *Phys. Rev. B: Condens. Matter Mater. Phys.* **1988**, *37*, 785−789.

(58) Ong, S. P.; Richards, W. D.; Jain, A.; Hautier, G.; Kocher, M.; Cholia, S.; Gunter, D.; Chevrier, V. L.; Persson, K. A.; Ceder, G. Python Materials Genomics (Pymatgen): A Robust, Open-Source Python Library for Materials Analysis. *Comput. Mater. Sci.* **2013**, *68*, 314−319.

(59) Auger, A.; Hansen, N. A Restart CMA Evolution Strategy with Increasing Population Size. *2005 IEEE Congress on Evolutionary Computation*, Edinburgh, Scotland, Sept 2−5, 2005; Vol. 2, pp 1769−1776.

(60) Tan, J.-C.; Civalleri, B.; Erba, A.; Albanese, E. Quantum Mechanical Predictions to Elucidate the Anisotropic Elastic Properties of Zeolitic Imidazolate Frameworks: ZIF-4 vs. ZIF-Zni. *CrystEngComm* **2015**, *17*, 375−382.

(61) Spencer, E. C.; Angel, R. J.; Ross, N. L.; Hanson, B. E.; Howard, J. A. K. Pressure- Induced Cooperative Bond Rearrangement in a Zinc Imidazolate Framework: A High- Pressure Single-Crystal X-Ray Diffraction Study. *J. Am. Chem. Soc.* **2009**, *131*, 4022−4026.

(62) Zheng, B.; Zhu, Y.; Fu, F.; Wang, L. L.; Wang, J.; Du, H. Theoretical Prediction of the Mechanical Properties of Zeolitic Imidazolate Frameworks (ZIFs). *RSC Adv.* **2017**, *7*, 41499−41503.

(63) Tan, J.-C.; Civalleri, B.; Lin, C.-C.; Valenzano, L.; Galvelis, R.; Chen, P.-F.; Ben-nett, T. D.; Mellot-Draznieks, C.; Zicovich-Wilson, C. M.; Cheetham, A. K. Exception- ally Low Shear Modulus in a Prototypical Imidazole-Based Metal-Organic Framework. *Phys. Rev. Lett.* **2012**, *108*, No. 095502.

(64) Chaplais, G.; Fraux, G.; Paillaud, J.-L.; Marichal, C.; Nouali, H.; Fuchs, A. H.; Coud- ert, F.-X.; Patarin, J. Impacts of the Imidazolate Linker Substitution (CH3, Cl, or Br) on the Structural and Adsorptive Properties of ZIF-8. *J. Phys. Chem. C* **2018**, *122*, 26945−26955.

(65) Amirjalayer, S.; Tafipolsky, M.; Schmid, R. Exploring Network Topologies of Copper Paddle Wheel Based Metal−Organic Frameworks with a First-Principles Derived Force Field. *J. Phys. Chem. C* **2011**, *115*, 15133−15139.

(66) Baburin, I. A.; Leoni, S.; Seifert, G. Enumeration of Not-Yet-Synthesized Zeolitic Zinc Imidazolate MOF Networks: A Topological and DFT Approach. *J. Phys. Chem. B* **2008**, *112*, 9437−9443.

■ NOTE ADDED IN PROOF

A related study by Weng and Schmidt was very recently published in *J. Phys. Chem. A* [DOI: 10.1021/acs.jp-ca.8b12311]. The authors developed a transferable ab initio intramolecular force field for ZIFs based on general Amber force field and reoptimized against DFT-calculated properties using a genetic algorithm.